Proceedings of the 28th IEEE
EMBS Annual International Conference
New York City, USA, Aug 30-Sept 3, 2006

Contrast Enhancement for Hypoechoic Lesions

Vincent Laurain and Dieter Hönigmann
Advanced Computer Vision GmbH - ACV, Vienna, Austria, e-mail: office@acv.ac.at

Abstract— **We propose a novel method for contrast enhancement in hypoechoic lesions. Our approach is based on the concept of distance on image manifolds to obtain a credibility function which captures the delineation of the lesion; if the lesion is sharply defined, the credibility function will also give a sharp response, whereas it varies smoothly at locations where no reliable information about the lesion's perimeter exists due to shortcomings of image acquisition, or because the lesion's border itself is only vaguely defined. The credibility function is used to either increase contrast of the lesion with respect to the adjacent tissue or to stain the lesion by a color overlay.**

I. Introduction

Ultrasound imaging is established as a valueable complement to mammography in the detection and classification of breast lesions. In this context, the assessment of the *mass margin*, *mass shape*, *pseudocapsule thickness*, *acoustic transmission* and *mass echogenicity* plays an important role in diagnosis [1], also comprising descriptors within the BI-RADS sonographic lexicon [2].

One specific way of assisting a clinician in diagnosis is the enhancement of contrast to improve the discriminability between the lesion and the adjacent tissue. Ultimately, a contrast enhancement technique of this type applied to an image showing just two different types of tissue would produce an image with only two intensity values: one of these values would be assigned to each pixel according to the tissue type it represents. One intermediate result of the approach we propose closely resembles such a bipartition of the image. However, it incorporates the concept of *uncertainty* in a way similar to our previous work in [3] in order to avoid enhancement of contrast at locations where either no reliable information exists due to shortcomings of image acquisition, or the lesion's border itself is only vaguely defined.

One of the most important requirements of an imaging system providing contrast enhancement is the preservation of the image characteristics. In the case of ultrasound data, the speckle nature of the images shall be retained. This property makes contrast enhancement a very difficult task. Thus standard methods for contrast enhancement such as *unsharp masking*, or *histogram equalization*[4] fail. More sophisticated methods based on *multiscale wavelet shrinkage techniques* [5], and *non-uniform* or *anisotropic diffusion* [6] can handle sonographic images but remove the speckle from the image and thus *do* change the characteristics of the image completely. The same is true for an approach suggested by Czerwinski et al. in [7]. The authors propose filtering the image with "sticks", short line segments which are varied in orientation to achieve the maximum projected value at each point. As an alternative to using the filtered image directly, they propose to use it for "staining" the original image by applying to each pixel a false color whose hue is related to the orientation of the most prominent line segment at that point. Staining works fine for hyperechoic structures, whereas it fails for hypoechoic lesions. In contrast, our approach enhances a lesion by *adding* color and / or contrast.

Finally, we aim at a solution operating in real-time, allowing contrast enhancement on-the-fly during the image acquisition and visualization process. Therefore, we employ techniques suitable for a highly efficient implementation such as a *Bayesian approach* and *distance transforms on image manifolds*.

II. Methods

We propose a method to enhance the contrast of hypoechoic lesions in B-mode ultrasound images. The goal is to preserve image characteristics while improving the discriminability of the lesion with respect to the adjacent tissue. The method comprises several steps:

1) Manual selection of one point p or a set of points $P = \{p_i\}, i \in \mathbb{N}$ within a lesion L;
2) Based upon P, computation of a distance function ϕ_P on an image manifold;
3) Determination of reference regions A and B, with $A \subseteq L$ and $B \subseteq \bar{L}$, with $\bar{L}$ denoting the complement of L;
4) Determination of a "credibility" function c by a Bayesian approach;
5) Enhancement of contrast based on c.

Let us start with a short review on the concept of distance on image manifolds.

A. Distance on Manifolds

The concept of image manifolds is well known in computer vision, see, e.g. [8] and [9]. To compute distance on image manifolds, an n-dimensional image comprising m-dimensional feature vectors is considered as an embedding $X : \Sigma \to M$ of an n-dimensional manifold Σ with coordinates $\sigma^1, \sigma^2, \cdots, \sigma^n$ in an $(n+m)$-dimensional hybrid space M of mixed spatial coordinates and feature coordinates $X^1, X^2, \cdots, X^{n+m}$. Here, we assume that the embedding space is Riemannian, i.e., in M there is locally an inner product defined by the metric $\mathbf{H}$, given by a symmetric positive definite matrix. Then the induced metric $\mathbf{G} = (g_{\mu\nu})$ of the Riemannian space $(\Sigma, \mathbf{G})$ is explicitly given by the symmetric positive definite matrix

$$g_{\mu\nu} = \left(\frac{\partial \mathbf{X}}{\partial \sigma^\mu}\right)^T \cdot \mathbf{H} \cdot \left(\frac{\partial \mathbf{X}}{\partial \sigma^\nu}\right). \quad (1)$$

1-4244-0033-3/06/$20.00 ©2006 IEEE.

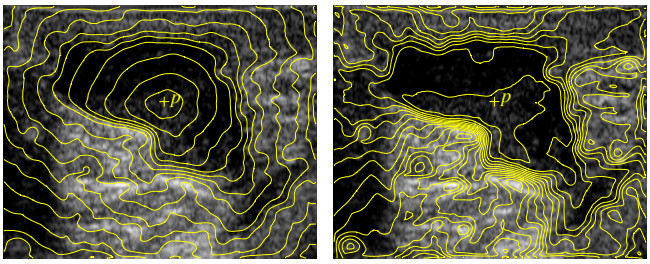

(a) (b)

Fig. 1. Given an image, the distance to p on the image manifold considers spatial distance to p resulting in level sets depicted in (a), while the distance function obtained by subtraction of the Euclidean distance does not, see (b).

In the present case of 2D intensity data $I(x,y)$, we employ an embedding of the form $(X^1,X^2,X^3) = (x,y,I(x,y))$. The metric of the embedding space $\mathbb{R}^3$ has been chosen to be the canonical Euclidean one, i.e., $\mathbf{H} = (h_{ij}) = \delta_{ij}$. Thus, the induced metric is

$$\mathbf{G} = \begin{pmatrix} 1+I_x^2 & I_xI_y \\ I_xI_y & 1+I_y^2 \end{pmatrix}. \tag{2}$$

Let ϕ be a function on Σ, i.e., a function in Σ's parameter space $D \subset \mathbb{R}^2$. The function describes a *distance function* on Σ iff its gradient with respect to the given metric is normalized. It is well known that this is precisely the case if the ordinary gradient $\nabla\phi$ satisfies the Hamilton-Jacobi equation

$$\nabla\phi^T \cdot \mathbf{G}^{-1} \cdot \nabla\phi = 1. \tag{3}$$

Given a point p in the parameter space D, we compute its image on the manifold Σ, and the distance function to p on Σ. The representation of that distance function in D will simply be called the distance function ϕ of p, denoted by ϕ_p. Given a set of points P, the distance function ϕ_P comprises for each pixel the shortest distance with respect to all $p_i \in P$. An efficient *fast sweeping* algorithm for solving (3) has been proposed by Tsai et al. in [10]. Prerequisite for applying *fast sweeping* for solving (3) is the smoothness of Σ. Considering the speckle prevalent in ultrasound data, we propose the embedding

$$(X^1,X^2,X^3) = (x,y,G*I(x,y)) \tag{4}$$

with G a 2D Gaussian kernel chosen to suppress speckle noise and $*$ denoting the convolution operator.

Due to (4) the resulting distance function ϕ considers both spatial distance as well as differences in intensities. Inside L, signal intensity does not change much, resulting in a distance function closely approximating the canonical Euclidean distance to P. At the border between lesion and tissue we expect an increasing signal intensity, resulting in a local increase of ϕ, see Fig. 1(a). In order to avoid a preference for circular shapes by the canonical Euclidean component introduced by the spatial components in (4), we "remove" the canonical Euclidean component by subtraction. The level sets of ϕ indicate that the underlying metric now considers image features only, see Fig. 1(b). Note that ϕ is different from $G*I(x,y)$ even after subtracting the canonical Euclidean component: it "integrates" intensity differences starting from P. Subsequently, we will use the distance function ϕ to obtain reference regions A and B, representing the lesion L and the embedding tissue $\bar{L}$, respectively.

B. Crater Distance Function

In addition to the given set of points P within the lesion L, we may automatically determine a set of points Q as reference points for the embedding tissue $\bar{L}$ by defining Q as being the image border pixels, under the assumption that L itself does not touch the border. Based upon P and Q, we may obtain reference regions A and B, representing the lesion L and the embedding tissue $\bar{L}$ in an optimal way, as follows. We compute the distance function $\phi_{P\cup Q}$ from the point set $P\cup Q$, which has local minima both at points $p \in P$, and at points $q \in Q$ at the image border. The graph of $\phi_{P\cup Q}$ resembles the crater of a volcano, thus we introduced the term *crater distance function* for $\phi_{P\cup Q}$, see Fig. 2(a). Consequently, the local maxima of $\phi_{P\cup Q}$ comprise points which have a large distance from both P and Q, i.e., points difficult to assign to L or $\bar{L}$. Because L is usually more homogeneous than $\bar{L}$, the local maxima of $\phi_{P\cup Q}$ will always be in $\bar{L}$, closely delimiting L. We employ the adaptive threshold

$$T = \{(x,y) | \phi_{P\cup Q}(x,y) < \text{mean}(\phi_{P\cup Q})\} \tag{5}$$

to determine point sets A and B comprising points sufficiently close to $P\cup Q$ which can be assigned to L and $\bar{L}$ reliably.

It is then easy to decide for every point $(x,y) \in T$ whether it is located closer to a point in P or a point in Q by computing the sign of the dot product between the gradient field of $\phi_{P\cup Q}$ and the position vector field with respect to the center of gravity $(x_0,y_0)^T$ of P,

$$\nabla\phi_{P\cup Q}(x,y) \cdot \begin{pmatrix} x-x_0 \\ y-y_0 \end{pmatrix}. \tag{6}$$

Points $(x,y) \in T$ closer to P comprise the reference set A, whereas points $(x,y) \in T$ closer to Q comprise the reference set B. Consequently, reference sets A and B are obtained from a single or few user input points P in a robust way.

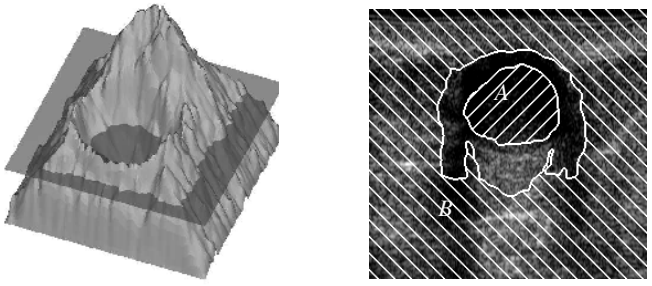

(a) (b)

Fig. 2. (a) Graph of the crater distance function $\phi_{P\cup Q}$ and threshold level. (b) We obtain reference regions A and B, superimposed onto the original image.

C. Credibility Function Inspired by Bayes' Equation

Bayes' theorem comprises the basis of Bayesian decision theory, a statistical approach to the problem of classification [11]. The Bayes equation links the posterior probability $p(\omega_j|x)$ of an event x to belong to a class ω_j among N classes, $j \in \{1..N\}$, to the likelihood $p(x|\omega_j)$ of each class ω_j. In the current scenario we assume the prior probabilities $p(\omega_j)$ are all equal to $1/N$ and can therefore be removed from the original Bayes equation which thus simplifies to

$$p(\omega_j|x) = \frac{p(x|\omega_j)}{\sum_{k=1}^{N} p(x|w_k)}. \tag{7}$$

Likelihoods $p(x|\omega_j)$ rely on probability models usually estimated for each class based on some reference data sets. As exposed in [11], using log-likelihood does not change the decision boundary between classes. Though, it serves to smooth $p(\omega_j|x)$, suiting better for *visualisation* purposes as pointed out in Fig. 3. For that purpose, the likelihood $p(x|\omega_j)$ is modeled by the Mahalanobis distance

$$D_M(x|\omega_j) = \frac{1}{2}(x-\mu_j)^t \Sigma_j^{-1}(x-\mu_j) + ln(|\Sigma_j|) \tag{8}$$

with μ_j the mean vector of the reference set for class j, Σ_j its covariance matrix, $|\Sigma_j|$ and Σ_j^{-1} its determinant and its inverse, respectively. In this application we consider two classes, ω_A and ω_B, with feature x defined as the distance function ϕ_P. Moreover, parameters Σ_j and μ_j, $j \in \{A,B\}$, are computed from ϕ_P on reference sets A and B, respectively. Finally, $p(\omega_A|x)$ is named credibility function $c(x,y)$ as it does not rely on a probability density distribution.

III. Results and Discussion

We once again want to point out that our goal is to enhance contrast strongly only at locations where there is both reliable information available, and the lesion's margin sharply defined.

In Fig. 4 we depict the original image and the credibility function $c(x,y)$. The latter exhibits different smoothness depending on the sharpness of the margin in the original data. If the margin is clearly defined, c decreases rapidly. However, it slowly fades if the margin is not clearly defined, e.g., in case of imaging artifacts such as shadows. In this case the lesion has the same echogenicity as the adjacent tissue in the B-image and it is the intensity variation caused by the speckle which provides increasing ϕ_P. Thus, using the distance function ϕ_P computed on the manifold rather than the original B-mode image intensities I allows differentiating between the lesion and adjacent tissue in this case.

There are different ways to enhance contrast based upon the credibility function c. On one hand, c can be used in a multiplicative way, i.e.,

$$E(x,y) = I(x,y)(1-c(x,y)). \tag{9}$$

The rightmost column in Fig. 4 shows the original data enhanced according to (9).

Alternatively, one can use c directly for "staining" I. We do that differently than proposed in [7], in order to increase discriminability of hypoechoic structures. Therefore we add a semitransparent layer additively, i.e.,

$$E(x,y) = I(x,y) + c(x,y). \tag{10}$$

This allows to display the original, unmodified B-mode image with a certainty image superimposed. The latter one can be switched on and off or dimmed gradually, providing additional insight into the lesions shape without obstructing the view on the B-mode image, see Fig. 5. We may as well employ different color maps in order to accentuate either the lesion's margin, or the entire lesion. Both ways of increasing the discriminability preserve the original structures and features of the B-mode image and add valueable information to aid the assessment of mass margin, shape, and the like.

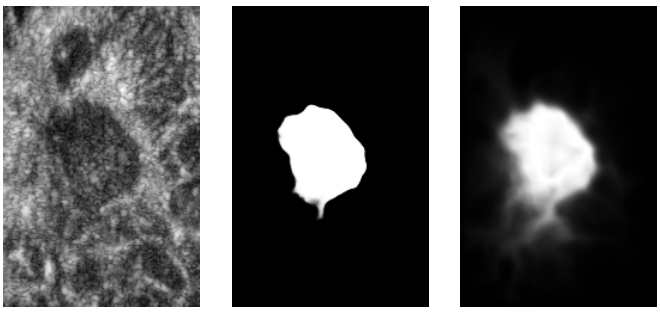

(a) (b) (c)

Fig. 3. (a) Original image; (b) $p(\omega_A|x)$ assuming Gaussian distribution for likelihood; (c) $p(\omega_A|x)$ based upon the Mahalanobis distance (credibility function c).

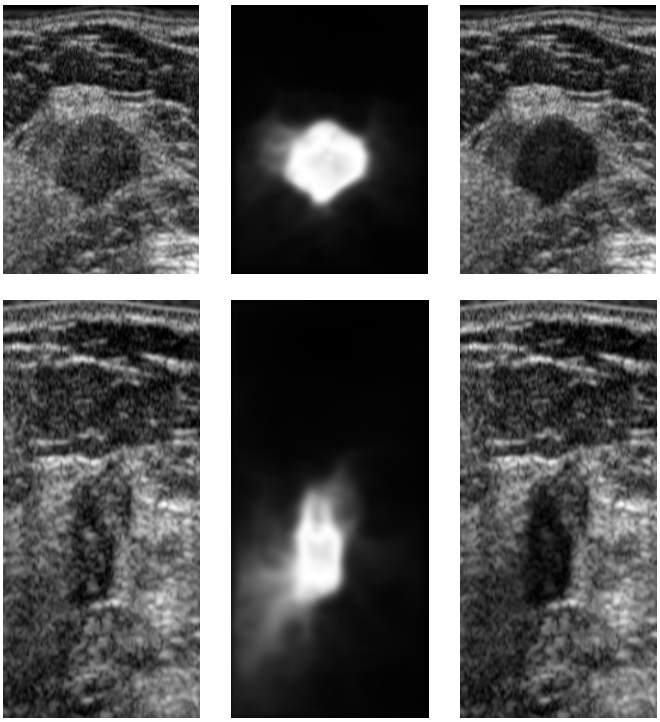

Fig. 4. Left: Original images. Center: Credibility function c. Right: Contrast enhanced according to (9).

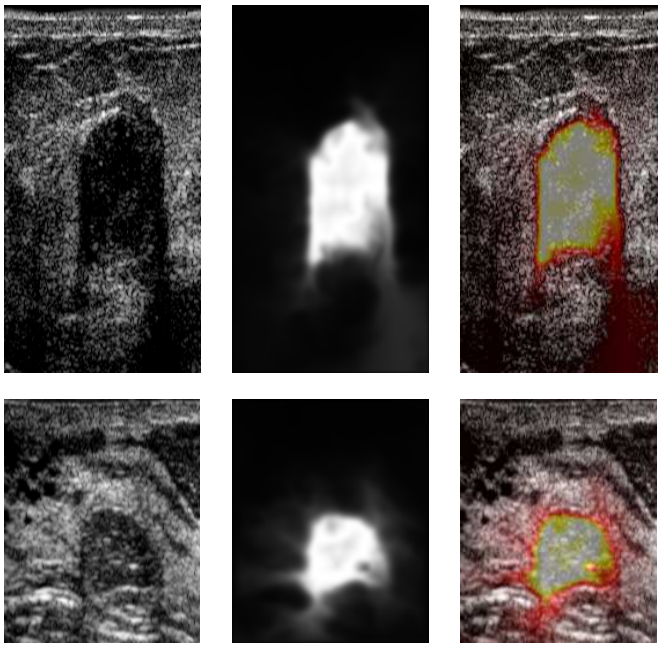

Fig. 5. Left: Original images. Center: Credibility function c. Right: Contrast enhanced according to (10). Here we used a color overlay which nicely emphasizes the lesions marginal areas.

Fig. 6 compares contrast enhancement of a B-mode image using posterior probabilities based on a Gaussian distribution in Fig. 6(b) and the Mahalanobis distance based credibility function c in Fig. 6(c). Enhancement in Fig. 6(b) creates artifacts in the image and can give a wrong clue concerning the mass' margin due to the "sharpness" of $p(\omega_A|x)$ at locations where the lesion's margin is not clearly defined.

For any contrast enhancement methodology dedicated for an interactive imaging modality like sonography real-time processing is absolutely necessary. An efficient implementation based on the SIMD capabilities of todays processors was realised and allows frame rates up to 25 frames per second, each comprising 300×300 pixels, on an Intel 2.3 GHz Pentium IV processor.

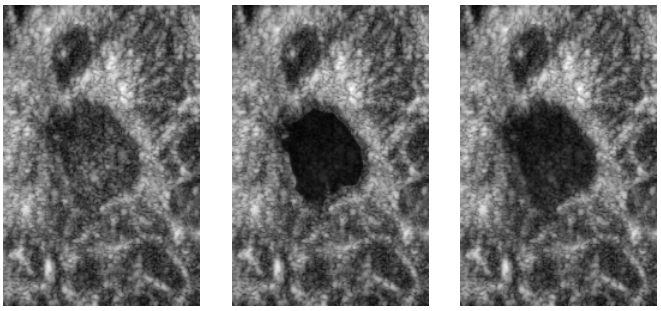

(a) (b) (c)

Fig. 6. (a) original images; (b) contrast enhancement using posterior probability based on gaussian distribution assumptions; (c) contrast enhancement using credibility c.

IV. Conclusions

We proposed a method for contrast enhancement of hypoechoic lesions in B-mode ultrasound data, requiring a minimal user interaction, based on the concept of distance functions on image manifolds and Bayes equation. We employ a distance function which efficiently and accurately provides reference regions required for estimating a credibility function, based on only a single, or a few, input points manually selected to indicate the hypoechoic structure of interest. Of course, one can imagine ways to determine these points automatically, but this is beyond the scope of the present paper.

The credibility function can be used directly for "staining" the original B-mode image, thus providing additional information without obstructing the view of the original image. On the other hand, it can also be used to increase contrast in the original image in a multiplicative way, without changing the typical feature of sonographic images used by physicians in diagnosis, such as speckle.

V. Acknowledgements

The authors would like to acknowledge the contributions of Armin Schoisswohl of GE Medical Systems Kretztechnik, Zipf, Austria, in providing the ultrasound data sets and valuable discussions. This work has been carried out within the K*plus* Competence Center ADVANCED COMPUTER VISION and was funded by the K*plus* program.

References

[1] A. T. Stavros, D. Thickman, and C. L. Rapp. Solid breast nodules: use of sonography to distinguish between benign and malignant lesions. *Radiology*, 196:123–134, 1995.

[2] A. S. Hong, E. L. Rosen, M. S. Soo, and J. A. Baker. Bi-rads for sonography. *American Journal of Roentgenology*, 184:1260–1265, 2005.

[3] B. Petersch, O. Serrano, and D. Hönigmann. 3d soft segmentation and visualization of medical data based on nonlinear diffusion and distance functions. In *EUROVIS06 Eurographics IEEE VGTC Symposium on Visualization*, pages 331–338. Eurographics Association, May 2006.

[4] M. Sonka, V. Hlavac, and R. Boyle. *Image Processing, Analysis, and Machine Vision*. PWS Publishing, Pacific Grove, CA, 2nd edition, 1999.

[5] X. Zong, A. F. Laine, and E. A. Geiser. Speckle reduction and contrast enhancement of echocardiograms via multiscale nonlinear processing. *Medical Imaging, IEEE Transactions on*, 17(4):532–540, 1998.

[6] J. Weickert. *Anisotropic Diffusion in Image Processing*. Teubner, Stuttgart, 1998.

[7] R. N. Czerwinski, D. L. Jones, and Jr. W. D. O'Brien. Detection of lines and boundaries in speckle images-application to medical ultrasound. *Medical Imaging, IEEE Transactions on*, 18(2):126–136, 1999.

[8] N. Sochen. A general framework for low level vision. *IEEE Transactions on Image Processing*, 7(3):310–318, 1998.

[9] R. Kimmel, R. Malladi, and N. Sochen. Images as embedded maps and minimal surfaces: movies, color, texture, and volumetric medical images. *International Journal of Computer Vision*, 39(2):111–129, 2000.

[10] Y. R. Tsai, L. T. Cheng, S. Osher, and H. K. Zhao. Fast sweeping algorithms for a class of hamilton-jacobi equations. *SIAM Journal on Numerical Analysis*, 41(2):673–694, 2003.

[11] R. O. Duda, P. E. Hart, and D. G. Stork. *Pattern Classification*. Wiley, New York, 2nd edition, 2001.